Available online at www.sciencedirect.com

ScienceDirect

Procedia CIRP 00 (2019) 000–000

www.elsevier.com/locate/procedia

53rd CIRP Conference on Manufacturing Systems

Milling stability identification using Bayesian machine learning

Jaydeep Karandikar[a], Andrew Honeycutt[a], Scott Smith[a], and Tony Schmitz[a,b]*

[a]*Energy and Transportation Science Division, Oak Ridge National Laboratory, Oak Ridge, TN 37830, USA*
[b]*Department of Mechanical, Aerospace, and Biomedical* Engineering, *University of Tennessee, Knoxville, Knoxville, TN 37996, USA*

* Corresponding author. Tel.: +1-865-974-6141; fax: +1-865-974-5274. *E-mail address:* tony.schmitz@utk.edu

Abstract

This paper describes automated identification of the milling stability boundary using Bayesian machine learning and experiments. The Bayesian machine learning process begins with the user's initial beliefs about milling stability. This "prior" is a distribution that uses all available information, which may be based only on experience or may be informed by physics-based model predictions. Experiments are then completed to update this prior by calculating the "posterior," a modified probabilistic description of the milling stability limit based on the new information. The approach is demonstrated and results are presented for both numerical and experimental cases.

Keywords: Machining; stability; artificial intelligence; machine learning; Bayes' rule

1. Introduction

High speed machining remains an important capability for discrete part manufacturing. To select operating parameters, the stability lobe diagram, which separates the stable axial depth of cut-spindle speed combinations from unstable (or chatter) combinations, may be used [1].

Nomenclature

A	uncertain event
B	experimental result
N	spindle speed
b	axial depth of cut
i	axial depth of cut grid point index
j	spindle speed grid point index
p	probability
s	stable
u	unstable
G	arbitrary grid point in the domain
T	test grid point
U_g	total grid uncertainty
+	stable result
-	unstable result
σ_N	standard deviation in spindle speed
σ_{NbT}	standard deviation in spindle speed at test axial depth
σ_b	standard deviation in axial depth of cut
K_s	specific cutting force coefficient

This manuscript has been authored by UT-Battelle, LLC under Contract No. DE-AC05-00OR22725 with the U.S. Department of Energy. The United States Government retains and the publisher, by accepting the article for publication, acknowledges that the United States Government retains a non-exclusive, paid-up, irrevocable, world-wide license to publish or reproduce the published form of this manuscript, or allow others to do so, for United States Government purposes. The Department of Energy will provide public access to these results of federally sponsored research in accordance with the DOE Public Access Plan (http://energy.gov/downloads/doe-public-access-plan).

The regeneration of surface waviness during material removal is the primary mechanism for chatter in machining [1-5]. Stability lobe diagrams enable the best spindle speeds to be selected that provide stable machining at increased axial depths of cut. These best spindle speeds occur where the tooth passing frequency is an integer fraction of the natural frequency that corresponds to the most flexible structural mode of vibration [1]. For a given tool-material combination, calculating the stability lobe diagram requires knowledge of the tool point frequency response function and the cutting force coefficients. These two input requirements can impose a significant hurdle for implementing the stability lobe diagram to maximize material removal rate in a production environment. Without knowledge of the tool point FRF and the cutting force coefficients, machining parameters are typically determined using tool supplier and handbook recommendations, or previous experience (i.e., what worked before). Furthermore, although analytical and numerical models exist to predict stability, they are typically treated as deterministic and do not consider the uncertainty in the stability boundary location due to uncertainties in the model inputs [6-8].

The objective of this study is to identify the stability boundary in a production environment by: 1) 'learning' the stability boundary using experimental results within a Bayesian updating framework; and 2) minimizing the number of required experiments. Previously, Karandikar *et al.* used a Bayesian random walk approach to identify optimal stable parameter combinations using profit as the objective function [9]. Li *et al* used an ensemble Markov Chain Monte Carlo method to update stability model parameters using experimental data [10]. Freidrich *et al* used online learning with a combination of reinforcement learning and nearest neighbor classification to determine the stability boundary [11]. There are two main contributions of this paper. First, a novel Bayesian learning approach to determine the stability boundary from experimental results is implemented by defining a prior and likelihood function that consider the underlying physics and the nature of the stability behavior. Second, an adaptive experimental strategy to identify the stability boundary is presented. The advantages of the proposed approach over the methods in the literature are: 1) the method works with and without an underlying stability model; 2) updating is possible with a single data point, and; 3) the method is computationally efficient. The remainder of the paper is organized as follows. Section 2 describes the Bayesian learning approach for stability boundary identification. Section 3 describes the experimental strategy for optimal parameter identification and the experimental results. Section 4 describes the influence of the prior. Conclusions are provided in Section 5.

2. Bayesian learning for milling stability

Bayes' rule offers a normative method for updating probabilities when new information is made available. Let $p(A)$ be the prior probability of an uncertain event A, $p(B \mid A)$ be the likelihood of obtaining an experimental result B given event A, and $p(B)$ be the probability of experimental result B. Bayes' rule calculates the posterior probability of event A given experimental result B, denoted by $p(A \mid B)$, as shown in Eq. 1.

$$p(A \mid B) = \frac{p(B \mid A)p(A)}{p(B)} \quad (1)$$

For milling stability, each axial depth-spindle speed combination is characterized using a probability of stability. The probability can be updated using Bayes' rule when experimental results are available. The prior represents the initial belief and is constructed by incorporating all available information (from analytical models, theoretical considerations, available experimental data, and expert opinions) [9]. Bayesian learning offers two main advantages. First, process knowledge can be incorporated in the prior and the likelihood functions. Second, the prior (or initial beliefs) can be updated using limited data, as opposed to the larger datasets required by neural networks or support vector machines, for example.

2.1 Constructing the prior

As noted, the prior represents the user's initial beliefs and can incorporate all available information. In the first portion of this study, it is assumed that the tool point FRF and the cutting force coefficients combination are not known. The prior probabilities are defined using only the knowledge that it is more likely to get an unstable cut as the axial depth is increased at any spindle speed. To illustrate, let the axial depth of cut, b, range be 0.01 mm to 20 mm and the spindle speed, N, range be 10000 rpm to 20000 rpm. The axial depth of cut and spindle speed range is divided into grid points where each grid point has a probability of being stable, s, denoted by $p(s)$, and a probability of being unstable, u, denoted by $p(u)$. As each grid point can either be stable or unstable, the sum of $p(s)$ and $p(u)$ is equal to 1. Figure 1 shows the prior probability of stability in the axial depth-spindle speed domain, where the colorbar denotes the probability of stability. It decreases linearly from 1 at an axial depth of cut equal to 0.01 mm to 0.05 at an axial depth of cut equal to 20 mm.

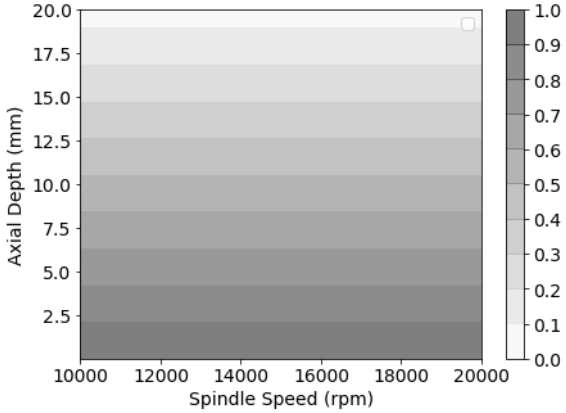

Figure 1. Prior probability of stability.

2.2 Bayesian updating at the test point using test result

Let a stable result test be denoted by '+' and an unstable test by '-'. Consider a stable result at the test grid point, denoted by T. The axial depth of cut and the spindle speed at the test point T are b_T and N_T, respectively. Equation 2 shows the application

of Bayes' rule to update the probability of stability at the test point for a stable test result at that point. In Eq. 2, $p(s_T)$ is the prior probability of stability at T, $p(+_T \mid s_T)$ is the likelihood probability of observing a stable result at T given that T is stable, and $p(+_T)$ is the probability of observing a stable result at T. The posterior probability of stability at T given a stable result at T is $p(s_T \mid +_T)$. The likelihood probability of observing a stable result at T given T is stable is 1. The probability of observing a stable result at T is calculated as shown in Eq. 3 using the law of total probability. In Eq. 3, $p(u_T)$ is the prior probability of T being unstable and $p(+_T \mid u_T)$ is the likelihood probability of a stable result at T given that T is unstable.

$$p(s_T|+_T) = \frac{p(+_T \mid s_T)p(s_T)}{p(+_T)} \tag{2}$$

$$p(+_T) = p(+_T \mid s_T)p(s_T) + p(+_T \mid u_T)p(u_T) \tag{3}$$

In Eq. 3, as stated, the likelihood probability of a stable result at T given that T is stable, $p(+_T \mid s_T)$, is equal to 1. The likelihood probability of a stable result at T given that T is unstable, $p(+_T \mid u_T)$, is equal to 0. Substituting the probability values in Eq. 2, the posterior probability of stability at T given stable result at T is 1, as shown in Eq. 4. Similarly, it can be shown that the posterior probability of stability at T given an unstable result at T, $p(s_T \mid -_T)$, is 0.

$$p(s_T \mid +_T) = \frac{1 \times p(s_T)}{1 \times p(s_T) + 0 \times p(u_T)} = 1 \tag{4}$$

2.3 Bayesian learning of stability in the axial depth-spindle speed domain

Bayes' rule can be used to update the probability of stability in the entire axial depth-spindle speed domain. The goal is to calculate the posterior probability of stability at each grid point given test result, stable or unstable, at T. Let G denote any arbitrary grid point in the axial depth-spindle speed domain. The axial depth of cut and the spindle speed at the grid point G are b_i and N_j, respectively, where i and j increments in the axial depth of cut range and the spindle speed range, respectively. Using Bayes' rule shown in Eq. 2, the objective is to determine probability of stability at G given test result at T (s_T is replaced by s_G). At the test point T, $b_i = b_T$ and $N_j = N_T$. To calculate the posterior probability of stability at each grid point, the likelihood probabilities, $p(+_T \mid s_G)$ and $p(+_T \mid u_G)$, need to be determined. If the likelihood probabilities, $p(+_T \mid s_G)$ and $p(+_T \mid u_G)$, are equal, the posterior probability is equal to the prior probability; see Eq. 2 and Eq. 3. The distance from the test point beyond which the likelihood probabilities are equal determines the influence of the test result in updating the probabilities of stability.

The first step is to calculate $p(+_T \mid s_G)$ and $p(+_T \mid u_G)$ as a function of the axial depth at the test spindle speed, N_T. At $b_i \leq b_T$, a stable result at T implies all axial depths of cut smaller than the test axial depth of cut are also stable; for simplicity, a stable result was added at smaller axial depths of cut. Therefore, at $b_i \leq b_T$, $p(+_T \mid s_G)$ was replaced by $p(+_G \mid s_G)$ which is equal to 1 and $p(+_T \mid u_G)$ was replaced by $p(+_G \mid u_G)$ which is equal to 0. At $b_i > b_T$, $p(+_T \mid s_G)$ is also 1, since if a grid point is known to be stable, a test at a smaller axial depth of cut will give a stable result with certainty. At $b_i > b_T$, $p(+_T \mid u_G)$ increases from 0. The influence of the stable test result at $b_i > b_T$ is defined using a standard deviation along the axial depth, denoted by σ_b. $p(+_T \mid u_G)$ is calculated using non-normalized Gaussian probability densities with $(b_T + 3\sigma_b)$ as the mean and σ_b as the standard deviation giving $p(+_T \mid u_G) = 1$ at $b_T + 3\sigma_b$. $p(+_T \mid u_G)$ is kept equal to 1 at $b_i > b_T + 3\sigma_b$; this ensures the posterior probability of stability equals the prior probability of stability at $b_i \geq b_T + 3\sigma_b$ and, therefore, the influence of the stable result is restricted to $b_T + 3\sigma_b$. $p(+_T \mid s_G)$ and $p(+_T \mid u_G)$ as a function of axial depth at N_T is given by Eq. 5 and Eq. 6, respectively:

$$p(+_T \mid s_G)_{N_T, b_i} = 1 \tag{5}$$

$$p(+_T \mid u_G)_{N_T, b_i} = \begin{cases} 0, & b_i \leq b_T \\ e^{-0.5\left(\frac{(b_i - (b_t + 3\sigma_b))}{\sigma_b}\right)^2}, & b_T < b_i \leq b_T + 3\sigma_b \\ 1, & b_i > b_T + 3\sigma_b \end{cases} \tag{6}$$

The influence of the test result along the spindle speed was defined by a Gaussian standard deviation, denoted by σ_N. The influence of a stable result increases at smaller axial depths of cut due to the nature of the stability lobe diagram where the width of the stability lobe increases at smaller axial depths. Therefore, σ_N is varied as a function of axial depth of cut. The influence of the test result along spindle speed at b_T, denoted by σ_{N_bT}, is first defined. At larger axial depth of cut values, σ_N value reduces linearly from σ_{N_bT} at b_T to zero at $b_T + 3\sigma_b$. At axial depths of cut smaller than b_T, σ_N increases at the same rate. Eq. 7 describes the relationship of σ_N as a function of the axial depth of cut for a stable test result.

$$\sigma_{N_{b_i}} = \begin{cases} -\frac{\sigma_{N_{b_T}}}{3\sigma_b} b_i + \frac{\sigma_{N_{b_T}}(b_T + 3\sigma_b)}{3\sigma_b} & b_i \leq b_T + 3\sigma_b \\ 0 & b_i > b_T + 3\sigma_b \end{cases} \tag{7}$$

At $b_i \leq b_T$, $p(+_T \mid s_G)$ is calculated using Gaussian probability densities with N_T as the mean and σ_N as the standard deviation, scaled between 0.5 to 1. A probability of 0.5 implies that it is equally likely to get a stable result or an unstable result at T given grid point is stable or unstable, implying maximum uncertainty. Since $p(+_T \mid u_G)$ increases from 0 along the spindle speed, it is calculated by subtracting $p(+_T \mid s_G)$ from 1. As a result, $p(+_T \mid s_G)$ and $p(+_T \mid u_G)$ converge to 0.5 at $N_T \pm 3\sigma_N$; this restricts the influence of the test result to $\pm 3\sigma_N$. $p(+_T \mid s_G)$ and $p(+_T \mid u_G)$ as a function of spindle speed at $b_i \leq b_T$ is given by Eq. 8 and Eq. 9, respectively.

$$p(+_T \mid s_G)_{N_j, b_i \leq b_T} = 0.5 + \frac{e^{-0.5\left(\frac{(N_j - N_t)}{\sigma_{N_{b_i}}}\right)^2}}{2} \tag{8}$$

$$p(+_T \mid u_G)_{N_j, b_i \leq b_T} = 1 - p(+_T \mid s_G)_{N_j, b_i \leq b_T} \tag{9}$$

As noted, at $b_i > b_T$, $p(+_T \mid s_G) = 1$ and $p(+_T \mid u_G)$ increases from 0 at b_T to 1 at $b_T + 3\sigma_b$ (Eqs. 5 and 6). $p(+_T \mid s_G)$ is calculated

as shown in Eq. 8. $p(+_T \mid u_G)$ is calculated by scaling the Gaussian probability densities between 0.5 to the likelihood value given by Eq. 6 for $p(+_T \mid u_G)$ as shown in Eq. 10.

$$p(+_T \mid u_G)_{N_j,\, b_i > b_T} = 0.5 + \frac{e^{-0.5\left(\frac{(N_j - N_t)}{\sigma_{N_{b_i}}}\right)^2}}{\left(\frac{1}{p(+_T \mid u_G)_{N_T,\, b_i > b_T}} - 0.5\right)} \quad (10)$$

The posterior probability of stability at each grid point is calculated from Eq. 2 and Eq. 3 using the prior probability of stability and the likelihood probabilities calculated using Eqs. 5-10. Figure 2 shows the posterior probability of stability in the defined axial depth-spindle speed domain given a stable result at T = {10 mm, 15000 rpm}; the filled 'o' denotes a stable result and the colorbar gives the probability of stability.

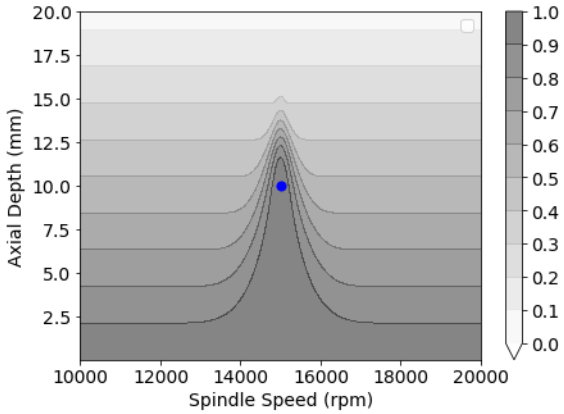

Figure 2. Posterior probability of stability given stable result at {10 mm, 15000 rpm}, denoted by the filled 'o'.

For an unstable cut, the likelihood probability values are the opposite of a stable result. An unstable cut implies that all axial depths of cut higher than the test axial depth of cut are also unstable. Therefore, at the test spindle speed, an unstable result can be added at each axial depth of cut higher than the test axial depth. At the test axial depth of cut, $p(-_T \mid s_G)$ increases from 0 to 0.5 and $p(-_T \mid u_G)$ reduces from 1 to 0.5 along the spindle speed. At axial depths less than the test axial depth, $p(-_T \mid u_G)$ is equal to 1 and $p(-_T \mid s_G)$ increases from 0 at b_T to 1 at b_T - $3\sigma_b$. σ_N increases linearly at $b_i > b_T$ with the same slope. Eqs. 5-10 would be modified for an unstable result and are not shown here for brevity. Figure 3 shows the updated probability of stability given an unstable result at {10 mm, 15000 rpm}; the 'x' denotes the unstable result.

3. Experimental validation

The Bayes' learning procedure for stability boundary identification was validated using experiments. As shown in Sections 2, each test result updates the probability of stability in the axial depth-spindle speed domain. The updated probability of stability is used to predict the stability boundary corresponding to a probability of stability equal to 0.5. A method to minimize the number of experiments required to identify the stability limit is as follows.

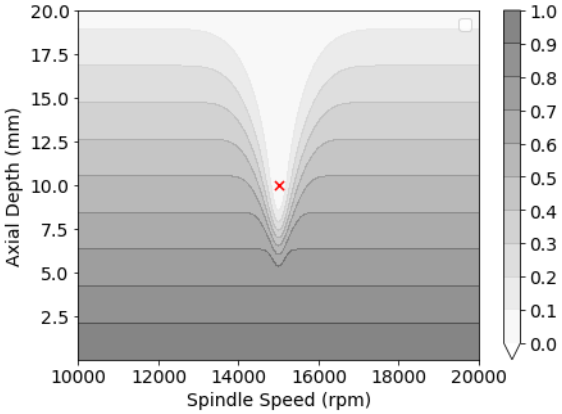

Figure 3. Posterior probability of stability given unstable result at {10 mm, 15000 rpm}, denoted by the 'x'.

To identify the stability limit, the objective is to reduce the uncertainty in the probability of stability at all grid points in the domain. If every grid point has a probability of stability equal to either 1 or 0, there is no uncertainty. In this case, the stability boundary will bisect the axial depths of cut where the probability of stability reduces from 1 to 0 at each spindle speed. If every grid point has a probability of stability equal to 0.5 (each grid point is equally likely to be stable or unstable), the uncertainty is maximum. In this case, a prediction of the stability boundary cannot be made. The uncertainty at a grid point is calculated as the minimum value from: $[1 - p(s_G), p(s_G) - 0]$. If the probability of stability at the grid point is either 1 or 0, the uncertainty at that grid point is 0. If the probability of stability at the grid point is 0.5, the uncertainty at that grid is maximum and equal to 0.5. The average total grid uncertainty, denoted by U_g, is defined as the average of the uncertainty at all individual grid points in the domain. The value of U_g ranges from 0 (where each grid point has a probability of stability equal to either 1 or 0) to 0.5 (where every grid point has a probability of stability equal to 0.5). Each experimental result (stable or unstable) updates the probability of stability at each grid point and therefore, reduces U_g. The optimal experimental parameters maximize the expected reduction in U_g after testing [12, 13]. The expected reduction in U_g after test at a grid point G is calculated as:

$$E[R(U_g)] = U_{g_{prior}} - \left(p(s_g)U_{g_s} + p(u_g)U_{g_u}\right) \quad (11)$$

In Eq. 11, $U_{g_{prior}}$ is the average grid uncertainty for the prior probability of stability, U_{g_s} and U_{g_u} is the average grid uncertainty calculated from the posterior probabilities of stability assuming G is stable and unstable, respectively. E is the expectation and R denotes reduction.

The experimental strategy was validated using experimental results. Milling tests were performed using a 12.7 mm diameter, four flute helical solid carbide endmill to machine a 6061-T6 aluminum workpiece. The axial depth of cut range and spindle speed range were selected as 0.01 mm to 4 mm and 6600 rpm to 10600 rpm, respectively. The experimental parameters were selected using the maximum expected reduction in U_g criterion described in Section 3. Before any experiments were performed, U_g was 0.256 for the prior shown in Fig. 1. For each experiment, the audio signal was recorded.

Stability was determined by converting the audio signal into the frequency domain using the Fast Fourier Transform (FFT) and by calculating the ratio of the chatter frequency amplitude to the largest amplitude among the fundamental tooth passing frequency and its harmonics, referred to as the stability ratio. If the stability ratio was greater than 0.5, the cut was considered unstable. Although other methods for determining machining stability have been developed, the stability ratio was applied in this study [14]. The test procedure was:

1. calculate the expected reduction in U_g at all grid points in the domain using Eq. 11;
2. select the spindle speed and axial depth combination where
3. the expected reduction in U_g is maximum;
4. perform test cut at the selected parameters;
5. record audio signal and determine if the test cut is stable and unstable
6. calculate posterior probability of stability based on the test result using the Bayesian learning procedure; posterior probabilities become prior for the subsequent update
7. repeat steps 1-5 for 20 tests.

For the updating procedure, σ_{NbT} and σ_b were selected as 120 rpm (3% of the spindle speed range) and 0.4 mm (10% of the axial depth of cut range), respectively. Figure 4 shows the updated probability of stability after 20 tests, where U_g reduces from 0.256 before any testing to 0.063 after 20 tests. Figure 5 shows the FFT of the audio signal for the experiment at {1.2 mm, 8600 rpm} and {2.1 mm, 9300 rpm}. At {1.2 mm, 8600 rpm}, chatter frequency is observed at 2065 Hz and the test was considered unstable. The results were validated by measuring the tool point FRF by tap testing and calculating the stability lobe diagram using the average tooth angle approach [1]. The cutting force coefficient was selected as 600 N/mm^2.

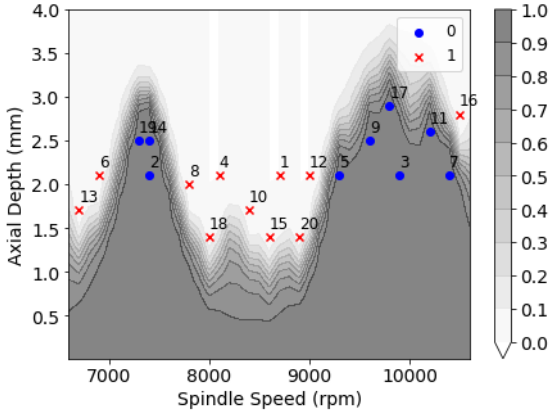

Figure 4. Posterior probability of stability after 20 tests.

Figure 6 compares the predicted stability boundary after 20 tests using the Bayes learning method and the analytical stability boundary. As seen from Fig. 6, the maximum expected reduction in U_g method identified several stable operating parameters in the stability lobes at 7400 rpm and 9800 rpm. The Bayes' learning method captures the nature of the underlying stability boundary as well as uncertainty in the stability prediction using the deterministic model. As seen from Fig. 6, the analytical lobe underpredicts the width of the stability limit at 9800 rpm. One limitation of the proposed experimental strategy is that the method is slow to converge to the stability boundary peak as seen at {9800 rpm, 3.9 mm} in Figure 6.

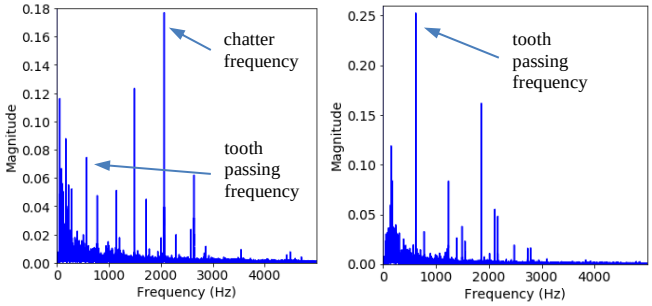

Figure 5. FFT for {1.2 mm, 8600 rpm} unstable test (left) and {2.1 mm, 9300 rpm} stable test (right); the chatter frequency for the unstable test is 2065 Hz.

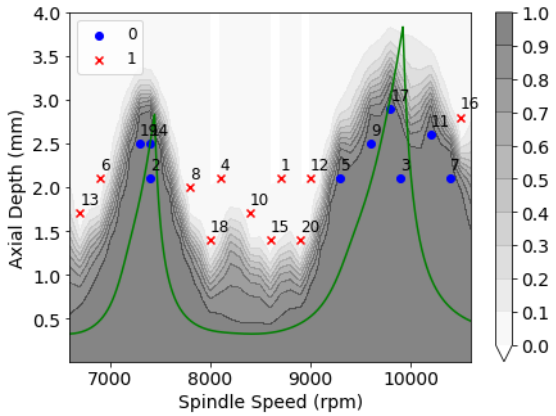

Figure 6. Posterior probability of stability after compared with analytical stability limit shown in solid line.

4. Influence of the prior

As noted, the prior represents the initial belief and is constructed by incorporating all available information. In the absence of knowledge of the FRF and the cutting force coefficients, the prior was based on the domain knowledge that it is more likely to get an unstable result as the axial depth increases at any spindle speed; see Fig. 1. If the FRF can be modeled (or measured), the prior can be generated by propagating the uncertainty in the model inputs through the stability model using a Monte Carlo simulation. The procedure is as follows. First, the tool point FRF was predicted using receptance coupling substructure analysis (RCSA). The details are provided in [1, 8, 15]. Given the predicted tool point FRF and assumed force model for the workpiece-tool pair, the corresponding stability limit was calculated using the frequency-domain analytical solution [1]. However, it was understood that both inputs included uncertainty. Therefore, mean values and standard deviations were selected to identify Gaussian distributions for the top uncertainty contributors: tool fluted diameter (standard deviation was 5% of the mean), tool stickout length (1%), carbide tool elastic modulus (5%), tool density (5%), connection stiffness and damping between the tool and holder (20%), and cutting force coefficients (20%). For each iteration in the Monte Carlo simulation, values for these uncertain variables were randomly selected, the tool point FRF was predicted, and a stability boundary was computed. At each grid point, the probability of stability was determined by calculating the fraction of the number of stability boundaries where the axial depth is greater than the grid point axial depth

at the same spindle speed. Figure 7 displays the prior probability of stability calculated using the Monte Carlo simulation, where U_g is equal to 0.114 for the informative prior. Figure 8 shows the posterior probabilities of stability after 20 tests, where U_g reduces from 0.114 before any testing to 0.042 after 20 tests. Comparing Figs. 6 and 8, beginning with the informative prior yields 17 stable tests and 3 unstable tests, while starting with the non-informative prior gives 9 stable and 11 unstable tests. As expected, an informative prior leads to a quicker convergence to the true stability boundary.

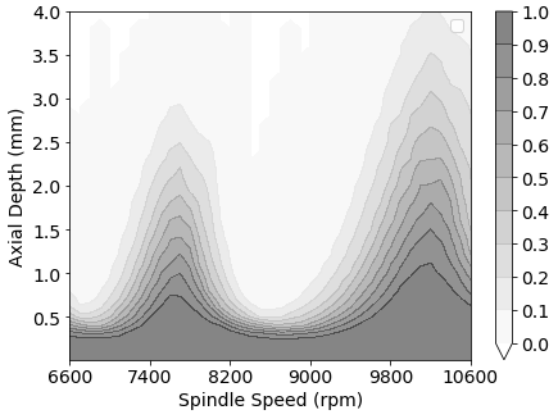

Figure 7. Prior probability of stability from the Monte-Carlo simulation

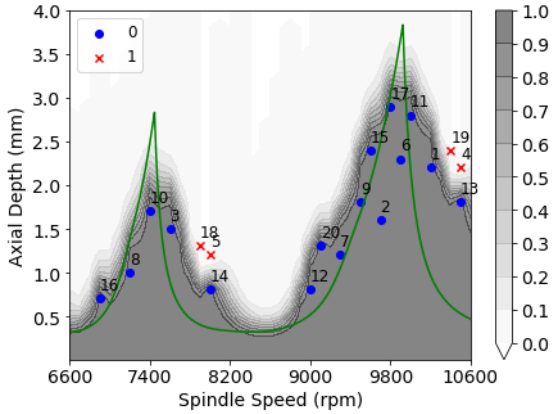

Figure 8. Posterior probability of stability after 20 tests using the maximum expected reduction in U_g criterion.

5. Conclusion

A novel Bayesian learning approach for stability limit prediction and optimal machining parameter identification was presented. The motivation for the approach was to enable learning of the stability boundary when the tool point frequency response function and cutting force coefficients are not known. The prior was selected based on the knowledge that at larger axial depths of cut, it is more likely to get an unstable result. Results showed that the Bayes' learning method was able to identify the stability boundary using test data. The Bayes' learning method does not require a large number of data points; a single test result updates the probability of stability. This enables continuous learning of the stability boundary in an industrial setting where large number of data points for every tool-material combination may not be available. As shown in Figure 4, 20 tests give a good prediction of the stability boundary for an uninformed prior.

An experimental strategy to optimize the selection of experimental parameters to identify the stability boundary using the maximum expected reduction in grid uncertainty was presented. Results showed that the method performs better than traditional grid-based design of experiment methods which are not adaptive and do not consider the experiment objective.

Acknowledgements

This research was supported by the DOE Office of Energy Efficiency and Renewable Energy (EERE), Energy and Transportation Science Division, and used resources at the Manufacturing Demonstration Facility, a DOE-EERE User Facility at Oak Ridge National Laboratory.

References

[1] Schmitz TL, Smith KS. Machining Dynamics: Frequency Response to Improved Productivity, Second Edition, Springer, New York, NY, 2019.
[2] Tlusty J. The stability of the machine tool against self-excited vibration in machining. Proc. Int. Res. in Production Engineering, Pittsburgh, ASME. 1963;465.
[3] Tobias SA, and Fishwick, W. Theory of Regenerative Machine Tool Chatter. The Engineer. 1958 Feb;205(7):199-203.
[4] Merritt HE. Theory of self-excited machine-tool chatter: Contribution to machine-tool chatter research—J. Eng. Ind. 1965;87(4):447–454.
[5] Arnold R. Cutting tools research: report of subcommittee on carbide tools: the mechanism of tool vibration in the cutting of steel. Proceedings of the Institution of Mechanical Engineers. 1946 Jun;154(1):261-84.
[6] Kim HS, Schmitz TL. Bivariate uncertainty analysis for impact testing. Measurement Science and Technology. 2007 Oct 4;18(11):3565.
[7] Duncan G, Schmitz TL, Kurdi MH. Uncertainty propagation for selected analytical milling stability limit analyses. Transactions of the NAMRI/SME; 2000. 34:17-24.
[8] Schmitz TL, Duncan GS. Three-point receptance coupling substructure analysis for tool point dynamics prediction. or tool point dynamics prediction. Journal of Manufacturing Science and Engineering. 2005 Nov 1;127(4):781-90.
[9] Karandikar J, Traverso M, Abbas A, Schmitz T. Bayesian inference for milling stability using a random walk approach. Journal of Manufacturing Science and Engineering. 2014 Jun 1;136(3):031015.
[10] Kai L, He S, Liu H, Mao X, Li B, Luo B. Bayesian uncertainty quantification and propagation for prediction of milling stability lobe. Mechanical Systems and Signal Processing 138 (2020): 106532.
[11] Friedrich J, Torzewski J, Verl A. Online learning of stability lobe diagrams in milling. Procedia CIRP. 2018 Jan 1;67:278-83.
[12] Howard RA. Information value theory. IEEE Transactions on systems science and cybernetics. 1966 Aug;2(1):22-6.
[13] Howard RA. Decision analysis: Perspectives on inference, decision, and experimentation. Proceedings of the IEEE. 1970 May;58(5):632-43.
[14] Rubeo M, Schmitz T. Amplitude ratio: A new metric for milling stability identification. Procedia Manufacturing. 2017;10:351-362.
[15] Schmitz TL, Donaldson RR. Predicting high-speed machining dynamics by substructure analysis. CIRP Annals. 2000 Jan 1;49(1):303-8.